Fault location in microgrids

A communication-based high-frequency impedance approach

Beheshtaein, Siavash; Cuzner, Robert; Savaghebi, Mehdi; Golestan, Saeed; Guerrero, Josep M.

Published in:
IET Generation, Transmission and Distribution

Publication date:
2019

Document Version
Accepted author manuscript, peer reviewed version

IET Generation, Transmission & Distribution

Fault Location in Microgrids: A Communication-based High-frequency Impedance Approach

Siavash Beheshtaein[1*], Robert Cuzner[2], Mehdi Savaghebi[1], Saeed Golestan[1], and Josep M. Guerrero[1],
[1] Department of Energy Technology, Aalborg, Denmark
[2] University of Wisconsin-Milwaukee, Wisconsin, USA
[*] sib@et.aau.dk

***Abstract*:** This paper proposes a novel method to locate faults in an AC meshed microgrid. To this end, a set of features is first extracted and selected from the measured signals and fed to a Support Vector Machine (SVM) to detect the occurrence of fault. Then, the Distributed Generator (DG) with the lowest amount of fundamental voltage, which is the closest one to the fault, injects an appropriate voltage/current harmonic. As the faulted section has the lowest impedance value from the PCC of the DG, the harmonic current of the corresponding line has the highest value. Based on this fact, the first candidate DG sends a notification signal to the second candidate DG, which the fault occurs between them. Finally, the impedances in the injected frequency are measured from these two DGs and fed into a multi-class SVM to locate the faulted line. The proposed method has the ability to locate faults for islanded and grid-connected microgrids with variable configurations. Real-time simulation results are taken by OPAL-RT to show the effectiveness of the proposed method in the meshed microgrid.
Keywords: Distribution Generations, Fault location, Microgrids, Protection.

1. Introduction

Microgrid, which consists of Distributed Generators (DGs), storage systems, and loads , is the backbone of a smart grid [1],[2]. In order to realize such a structure, many technical issues such as power quality, energy management, networked control, communication systems, and protection have to be addressed.

Microgrid should have a capability to operate in both islanded and grid-connected modes, and have a transition from grid-connected to islanded mode to protect itself from any disturbances [3]. In addition, the microgrid is required to reconfigure itself for economic reasons as well as for providing continuous electricity to essential loads [4]. Considering high integration of DGs, fault currents measured by protective relays significantly depend on microgrid configuration structure, operation modes, and existence of DGs in microgrid. Because of this, the protection of microgrid is probably the most important challenge for its realization [5],[6].

In the conventional radial distribution system, reclosers are used to allow existence of temporary faults with fuse protection if the fault persists [7]. In addition to recloser-fuse protection, overcurrent relaying is one of the most common approaches used in radial and meshed power networks, due to simplicity and low cost. However, high penetration of DGs could have adverse effects on the coordination of recloser-fuse and overcurrent relay approaches [8]. Distance protection, which measures impedance from the relay to the fault, will have a low selectivity in a microgrid with a high penetration of DGs. Besides, this protection demands a voltage transformer which results in a high implementation cost [9]. Similar to the distance relays, a directional relay involves a high implementation cost as it utilizes voltage and current transformers to determine the fault direction [10]. In addition, coordination of directional relays is difficult in multi-loop distribution systems. On the other hand, differential protection, which measures the currents flowing in and flowing out the bus, transformer, or transmission line to make decision for existence of fault, addresses the problems of bidirectional power flow and topology complexity, but implementation of a system having adequate discrimination capability is very costly [11].

In addition to the conventional relays, limiting the DG capacity [12], utilizing energy storage [13], Fault Current Limiter (FCL) [14], and adaptive protection [15],[16] have been presented to deal with the protection issues. The main drawbacks of these methods are, respectively, preventing high penetration of DGs due to high investment cost for DGs, high implementation cost of using FCLs and energy storage, and a need for a central unit for monitoring.

Typical microgrids operate in a radial fashion. However, meshed microgrid is a promising structure to realize a system with a higher resiliency and reliability by providing redundant paths [17]. It is shown that due to non-existence of the concept of upstream and downstream, the conventional protection would not work properly for the looped microgrid [18]. In such a microgrid, communication-based protection systems are better options for the detection and location of faults. In [19], differential relays are considered as the backbone of protection scheme; and in the case of communication channel failure, a comparative voltage protection is considered for the backup protection. In [20], a hierarchical protection scheme consisting of load-way level, loop-way level, feeder level, and microgrid level is proposed for the looped microgrid. Similar to [19], the differential protection is applied for distribution lines. This structure appears to be an effective option, particularly for looped microgrids, however, the implementation cost is high. In [21], the communication system is eliminated and in the case of fault, each DG changes its mode from the droop control mode to the current injection mode to provide a sufficient amount of current for overcurrent relays. The injected current of each DG is proportional to indirect measured impedance from the DG side. This method

may not correctly trigger circuit breakers in a system with different length of lines where DGs are located in short lines and the fault occurs in a long line. In addition, the performance of this method highly depends on the number of DGs and the fault impedance. On the other hand, it is preferred to eliminate the protection relays from the distribution lines [17]. Regarding this issue, the fault is located based on an approximated linear relationship between maximum oscillation of the transient voltage magnitude measured by a sensor and the distance between the fault location and the sensor [22]. However, this approach is not practical for the meshed microgrid.

This paper presents a new harmonic-injection based fault location method for meshed microgrid. This method utilizes control and power conversion capabilities inherent to the DGs (with some modifications) and only requires that each DG communicates with its adjacent DGs. In this method, the fault is locally diagnosed by extracting appropriate features from the currents and voltages of each DG and feeding them into a Support Vector Machine (SVM) classifier. While the fault is detected, first DG candidate is selected based on measuring fundamental voltage of DG terminal. Then, this DG injects the harmonic signal with a distinct high frequency and measures the high-frequency impedances of lines and according to these measurements another DG candidate, which are placed at the other side of faulty zone, is chosen. The second DG also injects a distinct high-frequency harmonic signal and measures the high-frequency impedance of line from its terminal. These measured harmonic impedances are considered in different topological configurations, such as grid-connected and islanded modes, as well as for various loads, DGs, and line disconnections; and fed into a Multi-class SVM (MSVM) to locate the faulty line in the meshed microgrid. Real-time simulation results are also provided to show the effectiveness of the proposed method.

2. Proposed Method

As mentioned in IEEE Std C37, a well-designed fault location method in ac transmission and distribution lines leads to rapid restoration of power systems. This standard classifies the fault location methods into impedance-based and traveling wave. These methods are implemented by microprocessor devices which have the requirements such as having the communication interface to transmit data to remote site and using digital filter for more accurate calculation. In addition, the central site collect the data and perform analysis to estimate the place where fault happens [23]. Regarding the hierarchical structure of microgrid, communication systems exist between the DG units for providing a proper control capability. In addition, the collected data in the primary level is transmit to the tertiary level, where database and computation center exist, for the purpose of optimization and better operation of microgrid [24].

Considering the requirements mentions by the IEEE Std C37 and the existing communication system as well as computation center in the microgrid, this paper proposes a fault location based on the existing infrastructure of microgrid. It must be noted that according to measured amplitude of signal by advanced phase locked loop communication link must transmit the data in synchronized way or in the worst case less than 20 ms delay to have proper outcome. In addition,

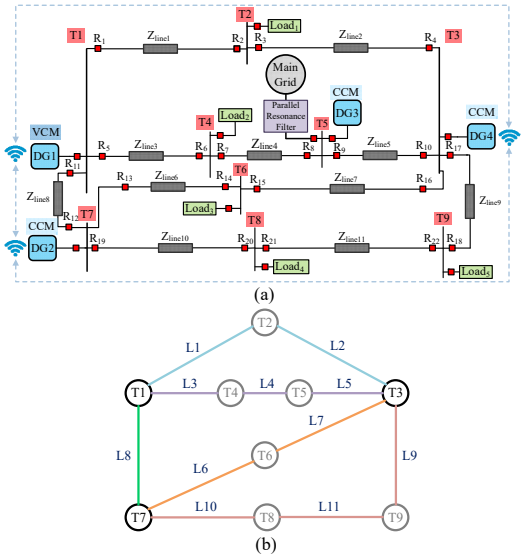

Fig. 1. *The meshed microgrid: (a) Scheme of the simulated microgrid, (b) Equivalent graph of the simulated meshed microgrid.*

the faulty section is determined in the tertiary level using the collected data from primary level.

Fig. 1(a) shows the proposed approach where high-frequency impedances are measured from two end-terminals of a faulty zone in a meshed microgrid. The microgrid could operate both in islanded and grid-connected modes. In the grid-connected mode, the voltage and frequency are maintained within an acceptable range by a stiff grid. However, in the absence of such a grid, at least one DG has to operate in Voltage Control Mode (VCM) to control voltage and frequency, and other DGs could work in Current Control Mode (CCM) [23]. The corresponding graph of Fig. 1(a) is shown in Fig. 1 (b). According to Fig. 1 (b), this connected graph has three vertices with a degree higher than two, T1, T3, and T7, as well as the others of degree two. The graph is partitioned to the edge disjoin paths whose endpoints are vertices with a degree higher than two. According to the above consideration, five subgraphs, which are shown in blue, purple, green, orange, and pink are respectively presented as follows:

$$
\begin{aligned}
&G_{zone1} = \{T_{zone1}, L_{zone1}\};\ T_{zone1} = \{T1, T2, T3\}; L_{zone1} = \{L1, L2\}\\
&G_{zone2} = \{T_{zone2}, L_{zone2}\}; T_{zone2}\ \{T1, T3, T4, T5\}; L_{zone2} = \{L3, L4, L5\}\\
&G_{zone3} = \{T_{zone3}, L_{zone3}\}; T_{zone3} = \{T1, T7\}; L_{zone3} = \{L8\}\\
&G_{zone4} = \{T_{zone4}, L_{zone4}\}; T_{zone4} = \{T3, T6, T7\}; L_{zone4} = \{L6, L7\}\\
&G_{zone5} = \{T_{zone5}, L_{zone5}\}; T_{zone5}\ \{T3, T7, T8, T9\}; L_{zone5} = \{L9, L10, L11\}
\end{aligned} \quad (1)
$$

According to the above way of partitioning, T1, T3, and T7 are the main nodes for creating subgraphs. From an electrical point of view, the existence of the DG1, DG2, and DG4 connected to the T1, T7, and T3 respectively, plays a

critical role in finding the faulty zone. Each defines a subgraph, and then the faulty line in the faulty zone.

Once the fault occurs in the microgrid, each DG investigates the occurrence of the fault by passing the selected features, which are extracted from output current of filter and voltage of DG's capacitor, to the SVM. When the fault is detected, two DG candidates, on each side of a fault location, must be chosen for locating the faulty line. The first DG candidate is the unit close to the faulty point and experiences the lowest amount of fundamental voltage. It must be noted that the comparison is carried out by using communication links between adjacent DGs (shown in Fig. 1(a)). This DG injects a high-frequency signal with a well-selected harmonic, and then from the connected terminal to this DG, the impedance is measured in that frequency. Based on the line that has the lowest high-frequency impedance/highest harmonic current in that high frequency, the faulty zone or subgraph where fault occurs is determined. As a result, the first DG candidate notifies the second candidate located on the other side of faulty zone by a communication link existing between these two DGs. While the second candidate receives the notification, it will inject another distinct high-frequency harmonic and impedance is measured associated with this harmonic. Finally, these two high-frequency harmonic impedances are fed into the MSVM to locate the faulty line. It must be noted that VCM DG has to exert a sufficient virtual impedance to block high-frequency signal generation by another DG. In addition, in order to prevent absorbing the high-frequency current by the main grid, a parallel resonance filter needs to be used. The whole procedure of the proposed protection is illustrated in Fig. 2. One of the key benefits of this method is its applicability for any type of complex microgrid structure.

2.1. Signal Processing Tools for Fault Detection and Location

An advanced signal processing method based on feature selection and the SVM/MSVM is used to detect the fault and locate it, described as follows:

2.1.1. Feature Extraction and Feature Selection

In addition to the amplitude of original signal, several features such as the standard deviation, RMS, and energy are extracted from the voltage/current of each phase of DG [25]. While the fault is detected, impedance of faulty zone is measured for the purpose of fault location:

$$Z^{high-frequency} = \frac{V^{high-frequency}{}_{faulty\,zone}}{I^{high-frequency}{}_{faulty\,zone}} \quad (2)$$

In order to increase the efficiency of classifier in terms of computational complexity, computation time, and accuracy, the most relative and informative subset of features have to be chosen. One of the widely used feature selection algorithms is the Sequential Forward Selection (SFS) algorithm that starts with an empty feature set and adds a feature to the set until no significant increase in accuracy occurs. This method is modified and the algorithm starts with the five best features and the conventional sequential forward selection algorithm is applied to each of five features. This process continues until accuracy of fault classification reaches a relatively fixed value.

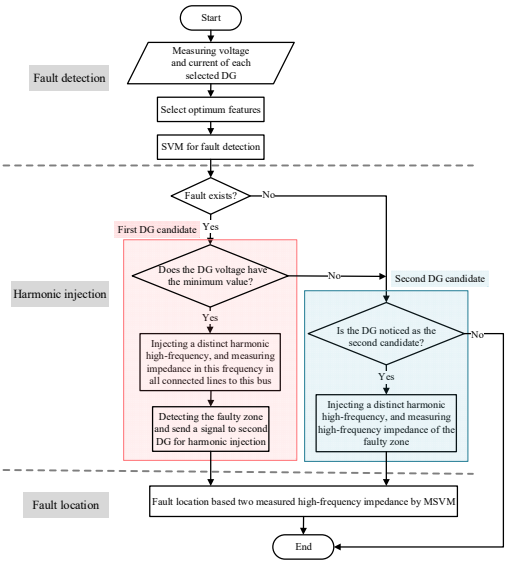

Fig. 2. *Flowchart of the proposed method.*

2.1.2. SVM

The SVM, which is a powerful binary classifier, adjusts a hyperplane to maximize the margin between two classes. This concept can be formulated as the following primal objective problem:

$$\min j(\omega,\zeta) = \left\{\frac{1}{2}\|\omega\|^2 + C\sum_{i=1}^{n}\zeta_i\right\}$$

Subject to: $y_i(\omega^T\phi(x_i)+b) \geq 1-\zeta_i, \zeta_i \geq 0, y_i = \{-1,+1\}^n,$
$\forall i = 1,2,\dots,n$ (3)

where ζ, C, $\varphi(x_i)$ and y_i are the deviation from the margin, penalty factor, a function that maps the testing data vector x_i onto high-dimensional feature space, and the corresponding label for each x_i, respectively. Typically, the primal form of SVM (3) is solved by transforming it to a dual form utilizing Lagrange multiplier method.

$$\min L(\alpha) = \left\{\frac{1}{2}\sum_{i=1}^{n}\sum_{i=1}^{n} y_i y_j \alpha_i \alpha_j K(x_i,x_j) - \sum_{i=1}^{n}\alpha_i\right\}$$
S.t. $\sum_{i=1}^{n}\alpha_i y_i = 0, 0 \leq \alpha_i \leq C\ \forall i = 1,2,\dots,n$ (4)

where α_i, N, and $\mathrm{K}(x_i,x_j) = \Phi(x_i)^T\Phi(x_i)$ are nonnegative Lagrangian multiplier, number of training data, and Kernel function, respectively. Among the different types of Kernel function, Gaussian Radial Basis Function (RBF) is selected, defined as follows:

$$K(x_i,x_j) = e^{-\gamma\|x_i-x_j\|^2} \quad (5)$$

where γ is the Kernel parameter.

The optimum decision function is achieved by solving this quadratic programming problem using training data with $\alpha_i^* > 0$ called support vectors [26].

$$g(x) = sign\left(\sum_{i\in SV} \alpha_i^* y_i K(x, x_i) + b^*\right) \quad (6)$$

$$b^* = \frac{1}{N_{SV}}\left(\sum_{i=1}^{N_{SV}} y_i - \sum_{i=1}^{N_{SV}} \alpha_j^* y_i K(x_i, x_j)\right) \quad (7)$$

Although the idea of SVM was first presented for binary classification, it can be applied for multiclass problems. One-against-all (OAA), one-against-one (OAO), and one-step (OS) are among the most practical methods to deal with multiclass problems. It is mentioned that OAO has more accuracy and low computation burden [27]. In OAO, n(n-1)/2 classifiers are constructed and trained for two classes, then the vote for i^{th} class is increased by one otherwise j^{th} class vote is added by one. Finally, the class with the highest vote wins.

2.1.3. Optimization of MSVM regarding feature selection

Particle Swarm Optimization (PSO) is one of the renowned evolutionary algorithms inspired by a flock of birds searching for food. Although each bird has its own velocity, the others movements can affect an individual bird's velocity and direction. Other behavioral stimulants such as inertia, cognitive stimulant, and social stimulant will be also influential [28]. According to the discussion above, the mathematical model for PSO is as follows:

$$V_i^{t+1} = \omega \times V_i^t + C_1 \times rand_1(.) \times (Pbest_i - X_i^t) + C_2 \times rand_2(.) \times (Gbest_i - X_i^t)$$
$$X_i^{t+1} = X_i^t + V_i^{t+1};$$
$$i = 1,2,3,\dots,N_{swarm} \quad (8)$$

where C_1, $C_2$are called learning factors and ω is inertia weight. In an original PSO algorithm, the above parameters remain constant. Inertia weight controls the next iteration speed. C_1 is considered as a cognitive parameter due to its ability to follow its own best value; however, C_2 is for tracking Gbest.

According to (6) and (7), C and γ need to be selected properly to give a high accuracy in the estimation of SVM classifier. In addition, an optimum number of features have to be selected. To attain these goals, the PSO algorithm is used to solve (3) and find the best set of features. The overall procedure is as follows:

Step 1: Take all the measured signals
Step 2: Extract features from the input signal.
Step 3: Select a feature of the input signal (It must not be in the Set With the Best-Selected Features (SWBSF)) and put it aside with the SWBSF.
Step 4: Optimize SVM by PSO algorithm to find the best C and γ regarding 10 fold-cross validation.
Step 5: Check the Step5 to Step 6 for all features that do not exist in the SWBSF. In addition, select and place the best of them in term of the lowest misclassification error in the SWBSF.
Step 6: If the classification accuracy does not change significantly, stop the process and choose the optimum C and γ, as well as SWBSF. Otherwise, go to Step 3.

2.2. Harmonic Injection

When the fault occurs in the meshed microgrid, its occurrence will be detected by the approach presented in the previous section. However, due to the meshed structure of microgrid, the faulted line is still unknown. To deal with this issue, while the fault is detected, two DGs placed at the beginning and the end of faulty zone inject voltage/current harmonic. As the fault causes voltage decrease in the meshed microgrid, one of the DG in faulty zone experiences the highest voltage drop. As a result, First DG is the one, which its fundamental voltage has the lowest value in comparison with adjacent DGs. Then, this DG injects a distinct high-frequency harmonic signal and measures the connected-lines impedances in that high frequency. Since the fault will result in low high-frequency impedance, the connected line with the lowest high-frequency impedance is part of the faulty zone. Based on this fact, the first DG identifies the second DG based on the line with the lowest high-frequency impedance, and sends a notification signal to the second one.

2.2.1. Harmonic Selection and Detection

Selecting frequency of harmonic components depends on different criteria such as having no interaction with the LCL filter resonant frequency, grid resonant frequency, and fundamental-frequency dependent harmonics (e.g. 5th, 7th,which are equal to 250 Hz and 350 Hz, respectively, in a 50 Hz system) [29]. This paper chooses 325 Hz, 275 Hz, and 375 Hz as appropriate frequencies for the injected signal by DG1, DG2, and DG4, respectively. In addition, according to the structure of the proposed method, both the fundamental and harmonic components of frequency 275 Hz, 325 Hz, and 375 Hz have to be detected. To address this issue, the present paper uses the Multiple Second-Order Generalized Integrators (MSOGI) based filter because of its good disturbance rejection capability, fast dynamic response and acceptable computational burden (see Fig. 3) [30].

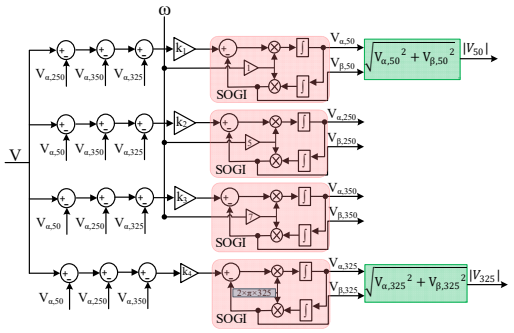

Fig.3. *MSOGI structure for fundamental and harmonic extraction of frequency 325 Hz.*

2.2.2. Control System

As mentioned before, microgrid may operate in both islanded and grid-connected modes. Such a microgrid requires both VCM and CCM DGs. The unit operating in VCM/grid forming is shown in Fig. 4 (a) and others in CCM/grid following are shown in Fig. 4 (b). As shown in Fig. 4 (a) and (b), the current and voltage harmonic references of 325 Hz are added to the generated fundamental current and voltage references, respectively. Since DG has to inject a harmonic of 325 Hz independently in each phase, the topology of DG must be three-phase four-wire. Among different topologies of four-wire systems, the three-leg inverter with split dc-link capacitors is popular where the midpoint of the split dc-link capacitors is connected to a neutral point [31].

As in the natural (abc) reference frame, a Proportional Resonance (PR) controller has a much better performance than PI regulator [32], PR controllers are considered in the inner control loops of both the VCM and CCM converters. Equation (10) describes PR controllers in the s-domain for the voltage and current control loops.

$$G_V = k_{PV} + \sum_{\substack{h=50,250,350,\\ 275,325,375}} \frac{2.k_{rVh}.\omega_{cV}.s}{(s^2 + 2.\omega_{cV}s + (\omega_h)^2)} \quad (9)$$

$$G_I = k_{PI} + \sum_{\substack{h=50,250,350,\\ 275,325,375}} \frac{2.k_{rIh}.\omega_{cI}.s}{(s^2 + 2.\omega_{cI}s + (\omega_h)^2)} \quad (10)$$

where, ω_{cV} ω_{cI}, and ω_h are the cut-off frequencies for current and voltage loops, and angular frequency for the related h, respectively. In addition, $k_V(k_I)$ and $k_{rV}(k_{rI})$ are proportional and resonant coefficients of the voltage (current), respectively. In the secondary control level, PI controllers are applied to generate proper control signals to restore both frequency and voltage to their nominal values. The related equations are as follows [32]:

$$\delta E = k_{PE}(E^*_{MG} - E_{MG}) + k_{iE}\int((E^*_{MG} - E_{MG}))dt \quad (11)$$

$$f = k_{Pf}(f^*_{MG} - f_{MG}) + k_{if}\int((f^*_{MG} - f_{MG}))dt \quad (12)$$

where, k_{PE}(k_{Pf}) and k_{iE}(k_{if}) are the parameters of PI controllers.

Once these correction values of voltage and frequency are obtained, these signals are sent to the primary control of each DG unit.

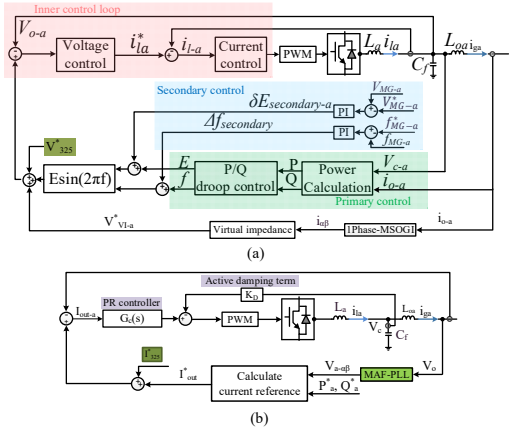

Fig.4. *Scheme of the control of phase-a of the three-phase four-wire DG with split dc capacitors. (a) VCM, (b) CCM*

As shown in Fig. 4 (b), for CCM-inverter the current reference is generated according to active and reactive powers references. Then, similar to VCM-inverter, the current error passes through PR controller defined as follows:

$$G_{CI} = k_{pII} + \sum_{\substack{h=50,250,350\\ 275,325,375}} \frac{2.k_{rIIh}.\omega_{cI}.s}{(s^2 + 2.\omega_{cI}s + (\omega_h)^2)} \quad (13)$$

2.2.3. Harmonic blocking for VCM-DG and main grid

The CCM-DG is modeled with a current source in parallel with a large impedance; however, the VCM-DG is modeled with a voltage source connected in series with a roughly low value impedance. Regarding this issue, the CCM-DG does not absorb any harmonic current, but the VCM-DG does. Absorption of harmonic current will deteriorate the performance of the proposed method, because it prevents flowing of current harmonics from the DG to the fault point. To deal with this issue, a high value of virtual impedance (VI) must be added for the specific harmonic components. As DG1 is adjacent to DG2 and DG4, where DG2 and DG4 generate harmonic signals at 275 Hz and 375 Hz respectively, DG1 has to block harmonics in these two frequencies by a well-designed VI. As shown in Fig. 5 (a), the single-phase MSOGI extracts harmonic components of output current in 50 Hz, 275Hz, and 375 Hz. Then, each of its current harmonic components is multiplied by a high virtual resistance. Finally, all these values are added together to generate an additional voltage reference and this term is added to the fundamental voltage reference (see Fig. 4 (a)).

In the grid-connected configuration, the main grid acts as a voltage source in series with the grid equivalent impedance. As a result, the main grid will absorb the harmonic signals injected by the DGs. In order to address this issue and let the high-frequency harmonic currents flow from DGs to the faulty point a parallel resonance filter is designed. Since the main grid is located between DG1 and DG4 that has a capability to

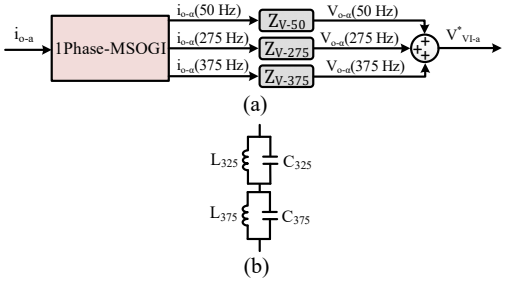

Fig.5. *Schematic diagram for blocking harmonic. (a) Virtual impedance, (b) Parallel resonance filter.*

inject harmonic signals in 325 Hz and 375 Hz, two parallel resonance filters are designed in series to block current harmonics in these two specific frequencies. The structure of parallel resonance filter with the capability of blocking harmonics of frequency 325 Hz as well as 375 Hz is shown in Fig. 5 (b).

3. Real-time Simulation Results

The meshed microgrid (Fig.1 (a)) with the parameters of Table 1 and Table 2 is implemented in Opal-RT with sampling time 20 ms to validate the effectiveness of the proposed method.

Table 1 Control parameters of the meshed microgrid.

Parameters	Symbol	Value
Voltage proportional term of VCM	k_{pV}	1
Voltage resonant term of VCM ($h=50$)	k_{rV50}	50
Voltage resonant term of VCM ($h\neq50$)	k_{rVh}	10
Current proportional term of VCM	k_{pI}	20
Current resonant term of VCM ($h=50$)	k_{rI}	1000
Current resonant term of VCM ($h\neq50$)	k_{iIh}	500
Cut-off frequency	ω_{cV}	2
Cut-off frequency	ω_{cI}	2
Current proportional term of CCM	k_{pII}	300
Current resonant term of CCM ($h=50$)	K_{rII50}	2500
Current resonant term of CCM ($h\neq50$)	k_{rIIh}	2500
Damping factor	K_D	300
Virtual resistance for 50 Hz	R_{v50}	4 Ω
Virtual for 275 Hz	R_{v275}	44 Ω
Virtual resistance for 325 Hz	R_{v325}	44 Ω
Active power droop term	k_{pP}	0.0003
Active power droop integral term	k_{iP}	0.0015
Reactive power droop term	k_{pQ}	0.2
Frequency proportional term	k_{pf}	0.01
Inductance for 325 Hz	L_{325}	0.2398 mH
Inductance for 375 Hz	L_{375}	0.1081 mH
Capacitance for 325 Hz	$C_{325,}$	1000 μF
Capacitance for 375 Hz	C_{375}	1000 μF

Table 2 Electrical parameters of the meshed microgrid.

Parameters	Symbol	Value
DC voltage	V_{dc}	650 V
Microgrid voltage	$V_{microgrid}$	311 V
Microgrid frequency	F	50 Hz
Filter capacitance	C	25 μF
Filter inductance	L	1.8 mH
Output inductance	L_o	1.8 mH
Constant active power load	P_{L1}	1500 W
Constant active power load	P_{L3}, P_{L4}	1000 W
Constant resistive load	R_{L2}, R_{L5}	70.53 Ω
Line resistance	$Z_{L1,}$ $Z_{L3,}$ $Z_{L4,}$ $Z_{L5,}$ $Z_{L6,}$ Z_{L7} $Z_{L8,}$ $Z_{L10,}$ Z_{L11}	1+j0.43 Ω
Line resistance	$Z_{L2,}$ Z_{L9}	2+j0.86 Ω

In order to demonstrate the efficiency of the proposed method, directional overcurrent relays (DOCRs) are coordinated by the concept of protection relay dependency dimension and primary protection relay set [33]. According to this method, {3,9,15,18} are selected as minimal breaking points (MBPS).Then these set of DOCRS including {3,1},{9,7,5,2},{15,13,20,22,17},{18,21,19,14,16},{18,21,19, ,11,2,4}, and {18,21,19,11,6,8,10} are coordinated. Regarding this method, two scenarios are considered to evaluate its performance. It must be noted it is assumed that these DOCRs adaptively change their setting for different possible scenario.

In the first scenario, as it is shown in Fig. 6, the main grid, DG3, Load2 are disconnected at 1.1s, 1.2s, and 1.3s, respectively. Then, a fault happens in line4 at 1.5s. As can be seen from the Fig. 6, the current measured by R7 and R8 increase from 0.5 A to 14.34 A and 12.06 A, respectively. And thanks to the proper coordination of the DOCRs, the associate circuit breakers of R7 and R8 disconnect the faulty line, which is line4, in 1.689s and 1.697s, respectively. In the second scenario, the main grid, load2 and DG3 are connected, and the fault occurs in line4 at 0.5s (see Fig. 7). In this scenario, the circuit breaker of R7 and R8 disconnect the line 4 at 0.5636 s and 0.7896 s, respectively. This method has two disadvantages, first, long operation time, which is due high numbers of DOCRs that need to be coordinated. Another one is that the parameters of DOCRs have to be tuned for each scenario.

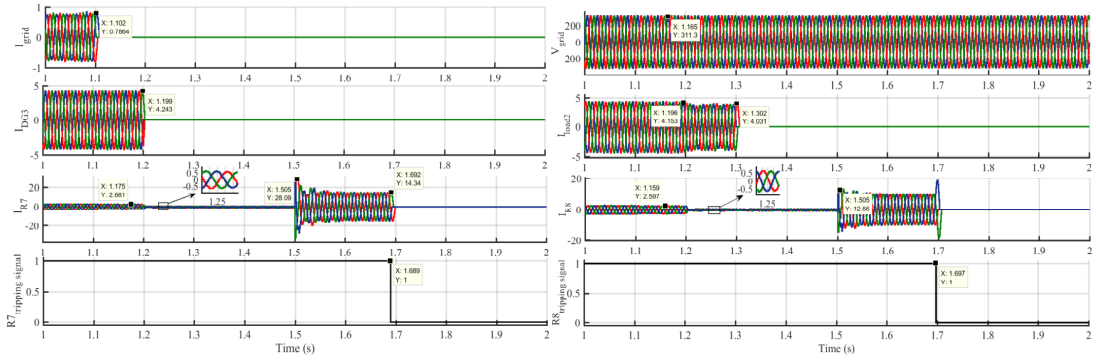

Fig. 6. *Real-time results for fault location in the meshed microgrid-scenarios 1 (regarding the adaptive DOCRs).*

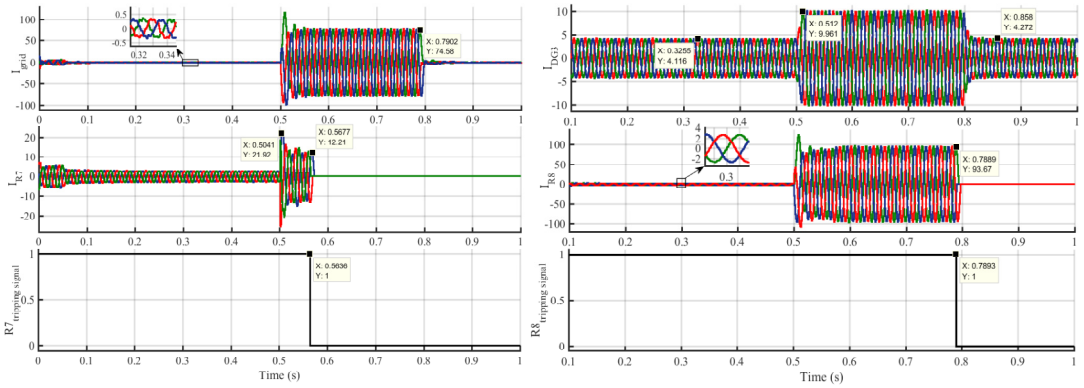

Fig. 7. *Real-time results for fault location in the meshed microgrid-scenarios 2 (regarding the adaptive DOCRs).*

Different scenarios including grid-connected and islanded modes, load connection/disconnection, line connection/disconnection, DG connection/disconnection, and different amount of fault resistances as well as fault locations are considered to validate the effectiveness of the proposed method.

In the first stage, fault has to be detected by selecting and feeding an appropriate set of features to the trained SVM. According to the modified SFS algorithm, the procedure of feature selection starts with the five best features and adds a new feature to each of those five until the classification accuracy reaches a fix value in the consecutive iterations. The obtained results presented in Table 3 show the first three iterations of the proposed feature selective algorithm in blue, pink, and green colors, respectively. According to this Table, the RMS values of three phases are selected as an appropriate set for feeding the SVM. The SVM with the parameters of C=10 and δ=45 is trained and tested with 450 data and 90 data, which include both faulty and normal situations, respectively. Although three features have been fed into the SVM, the 3D presentation of SVM hyperplane is not possible. Due to that, each pair of three selected features are fed to the trained SVM and shown in Fig. 8 (a).

From the selected buses two measured impedances in two distinct high-frequencies are fed to the MSVM to locate the faulty line. For example, in order to locate fault in Line4, Line5, and Line6, a MSVM with C=20 and δ=10 is trained and tested with two impedances measured in 325 Hz and 375 Hz from DG1 and DG4 for different scenarios. 750 scenarios as well as 300 scenarios including fault with different locations and fault resistances in these three lines are considered to train and test the MSVM, respectively. Fig. 8 (b) shows how the MSVM with inputs of the high-frequencies impendences can locate fault in each pair of lines. According to this figure, the faulty line is detected, regardless of the location.

Table 3 Feature selection for fault detection based on modified sequential forward algorithm.

Selected Features in each step	Class Type Accuracy	
	Normal	
std (I_a)	73.33 %	66.66 %
std (I_b)	73.33 %	66.66 %
RMS (V_c)	88.33 %	83.36 %
std (I_c)	73.33 %	66.66 %
Energy (V_b)	83.33 %	76.66 %
std (I_a), Inst. (V_a)	76.66 %	73.33 %
std (I_b), Inst. (V_a)	75 %	70 %
RMS (V_c), RMS (V_b)	93.33 %	90.33 %
std (I_c), std (I_a),	75 %	70 %
Energy (V_b), Energy (V_a)	86.66 %	76.66 %
std (I_a), Inst. (V_a), Inst. (V_c)	80 %	80 %
std (I_b), Inst. (V_a), Inst. (V_c)	76.66 %	73.33 %
RMS(V_c), RMS(V_b), RMS(V_a)	**100 %**	**100 %**
std (I_c), std (I_a), std (I_b)	81.66 %	83.33 %
Energy (V_b),Energy (V_a),Energy (V_c)	96.66 %	93.33 %

Regarding the trained SVMs for fault detection and fault location, different scenarios are applied to validate the effectiveness of the method presented in Fig. 2. In scenario 1 (see Fig.9), the microgrid transfers from grid connected to islanded mode in 1.1 s, then DG_3, line8, as well as $load_2$ get disconnected at 1.2 s, 1.3 s, and 1.4s, respectively. It must be emphasize that this scenario is taken into account to investigate the proposed method for the microgrid where its load, DG, and line get disconnected in grid-connected mode. In addition, in this scenario, the fault is exerted in the islanded microgrid, where such a stiff grid does not exist.

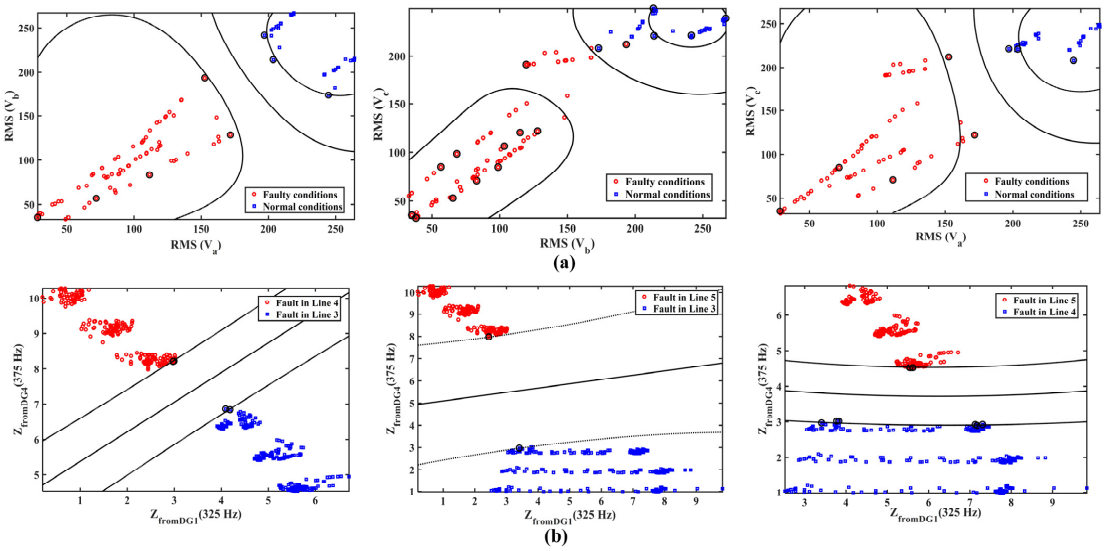

Fig. 8. *Trained SVM/MSVM classifier for fault detection and fault location: (a) The SVM for fault detection regarding each pair of feature, (b) The MSVM for fault location regarding pair of line.*

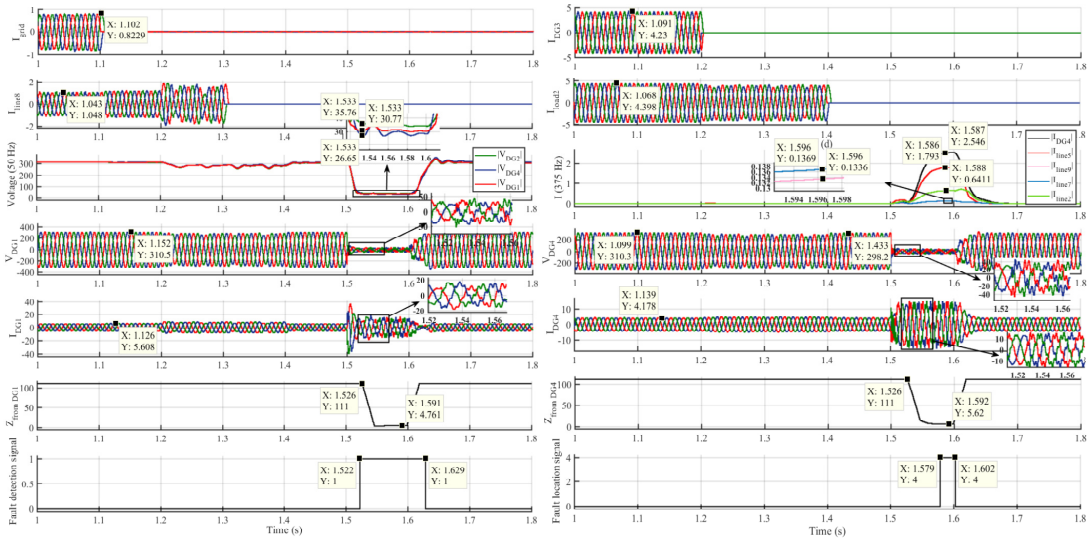

Fig. 9. *Real-time results for fault location in the meshed microgrid-scenarios 1 (regarding the proposed method)..*

As shown in Fig.9, the fault detection signal, which is generated by the trained SVM working online, does not change it status to the faulty situation during these scenarios. Finally, a three-phase fault to ground with R_f=0.0476 Ω occurs in Line4 at 1.5 s, after 22 ms (at 1.522 s) the fault is detected. While the fault is detected, amplitudes of DGs voltage (in 50 Hz) are compared and the DG with the lowest amplitude injects harmonic. Since DG4 has the lowest voltage amplitude with the value of 26.65 V, this DG injects a current harmonic of 375 Hz with the amplitude of 2.5 A. Fig. 9 show that this DG inject harmonic current around 1.53 s. Then, for the purpose of finding another DG candidate, which fault occurs between them, the current amplitudes of connected lines (in 375 Hz) are investigated. As the fault results in highest flow of harmonic current in the faulty zone, the connected line to DG4, here Line5, observes the highest harmonic current and based on this another DG candidate is selected. It must be noted again that the highest value of high- frequency harmonic current is identical to the lowest measured impedance in the applied high frequency. Regarding this issue, Fig. 9 shows that line5 has the highest harmonic current. As a result, DG1 is chosen as another candidate and this DG injects voltage

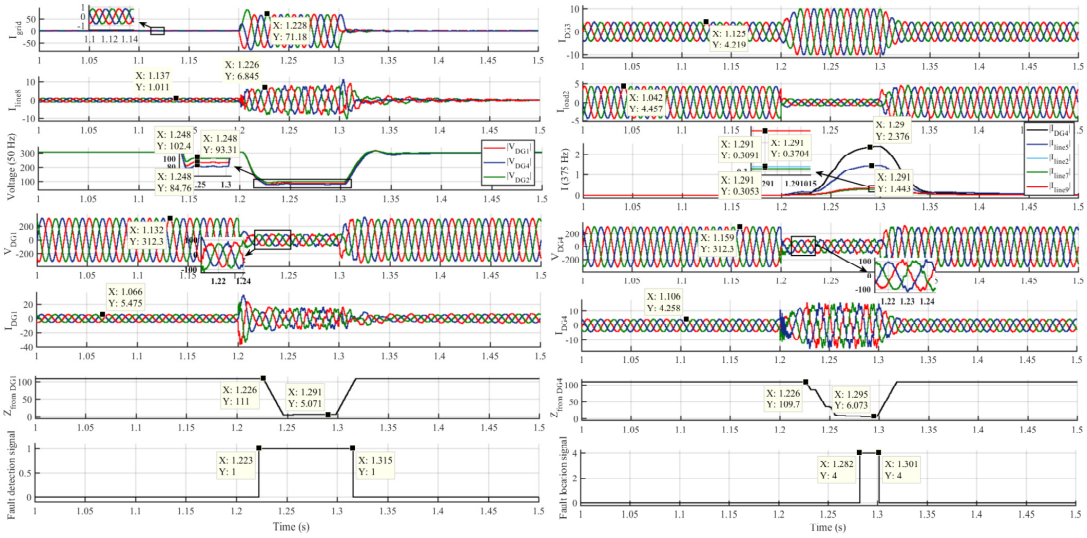

Fig. 10. *Real-time results for fault location in the meshed microgrid-scenarios 2 (regarding the proposed method).*

harmonic with 1/10 fundamental values (here around 5 V) in 325 Hz. Figs.7 show the voltage and current of DG1, where can be seen that applying voltage harmonic in 325 Hz leads to currents harmonic. It must be noted that all DGs limit current amplitude to 13 A to protect themselves from being damaged during the faulty conditions. After harmonic injection by the selected two DGs, the harmonic impedances are measured in 325 Hz and 375 Hz from DG1 and DG4, respectively. Based on the measured values from DG1 and DG4, the trained MSVM detect the faulty line, Line4 which is represented by number 4 in Fig. 9, after 80 ms from occurrence of the fault at 1.579 s. While the location of faulty line is detected, the tripping signal will be sent to the related circuit breakers, which are located at the beginning and the end of Line4, for fault isolation after 20 ms.

In scenario 2, microgrid operates in grid-connected mode and all DGs, loads, and lines are connected. In this case, a three-phase to ground fault with R_f=0.48 Ω takes place in Line4 at 1.2 s. As shown in Fig. 10, during the faulty situation the load current is decreased because this load is constant impedance with the value of R_{load2}=70.53 Ω. While the fault occurs, the SVM trained for fault detection detects fault in 22.3 ms (see Fig. 10). All voltages of DG1, DG2, and DG4 are compared to find the one with the lowest fundamental value. According to the Fig. 10, DG4 has the lowest voltage amplitude and this DG will send harmonic currents in 375 Hz with the amplitude of 2.5 A. In order to find the second DG candidate that fault occurs between that and the first candidate, the amplitudes of harmonic currents of all connected lines to DG4 are investigated. Since Line5 has the highest harmonic current in 375 Hz, DG1 will be chosen as the second candidate. This DG will inject harmonic voltage, because it is controlled in VCM, with 1/10 of the fundamental value of voltage. Fig. 10 shows the voltage and current signals of DG1. As it can be observed, voltage harmonic is injected at around 1.3 s. The impedances with the values of 5.071 Ω and 6.073 Ω are measured in 325 Hz and 375 Hz from DG1 and DG4 (the two candidate DGs), respectively. These two values are then fed to the trained MSVM to detect the faulty line, which is connected between these two DGs. As shown in Fig. 8, the trained MSVM finds the fault occurs in Line4, which is represented by number 4, after 82 ms from occurrence of the fault.

4. Conclusion

In this paper, a communication-based high-frequency impedance method is proposed for AC meshed microgrids. The functionality of this protective scheme is distributed among the DGs connected in microgrid, so that selected DGs take the responsibility of harmonic injection for the purpose of fault location. The main advantage of the proposed method is elimination of line relays and determination of the faulty line based on only measuring the voltage and current of DGs and the lines connected to them. In addition, this protection system is robust against change of microgrid operation mode, load connection/disconnection, line connection/disconnection, and DG connection/disconnection. In others word, the change in topology of microgrid does not affect the performance of the proposed protection system. In order to evaluate the efficiency of the proposed method, two different scenarios are considered. It is shown that in both scenarios, the fault is detected in around 20 ms, and based on strategy of harmonic injection by DGs, the faulty line is located in 80 ms.

Although this method has superior performance in term of speed, and be high efficient in different configuration and topology of the microgrids. The application of the proposed method in some scenarios may involve some difficulties. For example, it requires a communication system and demands designing advanced signal processing/filtering techniques, which may not be a trivial task, particularly for those who are not expert in the field.

5. References

1 Zadsar, M., Haghifam, M.R., Miri Larimi, S.M.:

'Approach for self-healing resilient operation of active distribution network with microgrid'*IET Gener. Transm. Distrib.*, 2017, **11**, (18), pp. 4633–4643.

2 Guerrero, J.M., Chandorkar, M., Lee, T., Loh, P.C.: 'Advanced Control Architectures for Intelligent Microgrids — Part I : Decentralized and Hierarchical Control'*IEEE Trans. Ind. Electron.*, 2013, **60**, (4), pp. 1254–1262.

3 Manaffam, S., Talebi, M., Jain, A.K., Behal, A.: 'Intelligent Pinning Based Cooperative Secondary Control of Distributed Generators for Microgrid in Islanding Operation Mode'*IEEE Trans. Power Syst.*, 2017, **33**, (2), pp. 1364–1373.

4 Tan, S., Xu, J.X., Panda, S.K.: 'Optimization of distribution network incorporating distributed generators: An integrated approach'*IEEE Trans. Power Syst.*, 2013, **28**, (3), pp. 2421–2432.

5 Che, L., Khodayar, M.E., Shahidehpour, M.: 'Adaptive Protection System for Microgrids: Protection practices of a functional microgrid system.'*IEEE Electrif. Mag.*, 2014, **2**, (1), pp. 66–80.

6 Piesciorovsky, E.C., Schulz, N.N.: 'Fuse relay adaptive overcurrent protection scheme for microgrid with distributed generators'*IET Gener. Transm. Distrib.*, 2017, **11**, (2), pp. 540–549.

7 Yazdanpanahi, H., Li, Y.W., Xu, W.: 'A new control strategy to mitigate the impact of inverter-based DGs on protection system'*IEEE Trans. Smart Grid*, 2012, **3**, (3), pp. 1427–1436.

8 Beheshtaein, S., Savaghebi, M., Vasquez, J.C., Guerrero, J.M.: 'Protection of AC and DC Microgrids : Challenges , Solutions and Future Trends', in 'Proc. 41th Annu. Conf. IEEE Ind. Electron. Soc. (IECON)' (2015), pp. 5253–5260

9 Brearley, B.J., Prabu, R.R.: 'A review on issues and approaches for microgrid protection'*Renew. Sustain. Energy Rev.*, 2017, **67**, pp. 988–997.

10 Chen, M., Shi, D., Duan, X.: 'Minimum break relay dependency set approach for coordination of directional relays in multi-loop networks'*IET Gener. Transm. Distrib. Res.*, 2017, **11**, (5), pp. 1279–1285.

11 Monadi, M., Zamani, M.A., Ignacio, J., Luna, A., Rodriguez, P.: 'Protection of AC and DC distribution systems Embedding distributed energy resources : A comparative review and analysis'2015, **51**, pp. 1578–1593.

12 Zeineldin, H.H., El-Saadany, E.F., Salama, M.M., Kasem Alaboudy, A.H., Woon, W.L.: 'Optimal sizing of thyristor-controlled impedance for smart grids with multiple configurations'*IEEE Trans. Smart Grid*, 2011, **2**, (3), pp. 528–537.

13 Jayawarna, N., Jones, C., Jenkins, N., Barnes, M.: 'Operating MicroGrid Energy Storage Control during Network Faults', in 'System of Systems Engineering' (2007), pp. 1–7

14 El-Khattam, W., Sidhu, T.S.: 'Restoration of Directional Overcurrent Relay Coordination in Distributed Generation Systems Utilizing Fault Current Limiter'*IEEE Trans. Power Deliv.*, 2008, **23**, (2), pp. 576–585.

15 Brahma, S.M., Girgis, A.A.: 'Development of Adaptive Protection Scheme for Distribution Systems with High Penetration of Distributed Generation'*IEEE Trans. Power Deliv.*, 2004, **19**, (1), pp. 56–63.

16 Mahat, P., Chen, Z., Bak-Jensen, B., Bak, C.L.: 'A simple adaptive overcurrent protection of distribution systems with distributed generation'*IEEE Trans. Smart Grid*, 2011, **2**, (3), pp. 428–437.

17 Che, L., Zhang, X., Shahidehpour, M., Alabdulwahab, A., Al-turki, Y.: 'Optimal Planning of Loop-Based Microgrid Topology'*IEEE Trans. Smart Grid*, 2016, pp. 1–11.

18 Prasai, A., Du, Y., Paquette, A., Buck, E., Harley, R.: 'Protection of Meshed Microgrids with Communication Overlay', in 'IEEE Energy Conversion Congress and Exposition' (2010), pp. 64–71

19 Sortomme, E., Venkata, S.S., Mitra, J.: 'Microgrid Protection Using Communication-Assisted Digital Relays'*IEEE Trans. Power Del.*, 2010, **25**, (4), pp. 2789–2796.

20 Rocabert, J., Luna, A., Blaabjerg, F., Paper, I.: 'Control of Power Converters in AC Microgrids'*IEEE Trans. Power Electron.*, 2012, **27**, (11), pp. 4734–4749.

21 Oureilidis, K.O., Demoulias, C.S., Member, S.: 'A Fault Clearing Method in Converter-Dominated Microgrids With Conventional Protection Means'*IEEE trans. Power Elecron.*, 2016, **31**, (6), pp. 4628–4640.

22 Microgrids, S.: 'A Novel Method of Fault Location for single-phase microgrids'*IEEE Trans. Smart Grid*, 2016, **7**, (2), pp. 915–925.

23 '"IEEE Guide for Determining Fault Location on AC Transmission and Distribution Lines, IEEE Standard C37.114"' (2014)

24 Meng, L., Luna, A., Díaz, E.R., *et al.*: 'Flexible System Integration and Advanced Hierarchical Control Architectures in the Microgrid Research Laboratory of Aalborg University'*IEEE Trans. Ind. Appl.*, 2016, **52**, (2), pp. 1736–1749.

25 Beheshtaein, S.: 'Application of wavelet-base method and DT in detection of ferroresonance from other transient phenomena', in 'International Symposium on INovations in Intelligent SysTems and Applications (INISTA)' (2012), pp. 1–7

26 Livani, H., Member, S., Evrenosoglu, C.Y., Member, S.: 'A Machine Learning and Wavelet-Based Fault Location Method for Hybrid Transmission Lines'*IEEE Trans. Smart Grid*, 2014, **5**, (1), pp. 51–59.

27 Hsu, C., Lin, C.: 'A Comparison of Methods for Multiclass Support Vector Machines'*IEEE Trans. Neural Networks*, 2002, **13**, (2), pp. 415–425.

28 Beheshtaein, S., Savaghebi, M., Guerrero, J.M.: 'A Fuzzy-based Hybrid PLL Scheme for Abnormal Grid Conditions', in 'Proc. Ind. Electron. Soc. Conf.' (2015), pp. 5095–5100

29 Reigosa, D.D., Briz, F., Member, S., Charro, C.B., García, P., Guerrero, J.M.: 'Active Islanding Detection Using High-Frequency Signal Injection'*IEEE Trans. Ind. Appl.*, 2012, **48**, (5), pp.

1588–1597.
30 Rodríguez, P., Member, S., Luna, A., *et al.*: 'Multiresonant Frequency-Locked Loop for Grid Synchronization of Power Converters Under Distorted Grid Conditions'*IEEE Trans. Ind. Electron.*, 2011, **58**, (1), pp. 127–138.
31 Verdelho, P., Marques, G.D.: 'Four-Wire Current-Regulated PWM Voltage Converter'*IEEE Trans. Ind. Electron.*, 1998, **45**, (5), pp. 761–770.
32 Savaghebi, M., Member, S., Jalilian, A., Vasquez, J.C., Guerrero, J.M., Member, S.: 'Secondary Control for Voltage Quality Enhancement in Microgrids'*IEEE Trans. Smart Grid*, 2012, **3**, (4), pp. 1893–1902.
33 Yue, Q., Lu, F., Yu, W., Wang, J.: 'A Novel Algorithm to Determine Minimum Break Point Set for Optimum Cooperation of Directional Protection Relays in Multiloop Networks'*IEEE Trans. Power Del.*, 2006, **21**, (3), pp. 1114–1119.